The Journal of Chemical Physics

Modeling oil–water separation with controlled wetting properties

Cite as: J. Chem. Phys. **154**, 104704 (2021); https://doi.org/10.1063/5.0041070
Submitted: 18 December 2020 . Accepted: 17 February 2021 . Published Online: 08 March 2021

Cristina Gavazzoni, Marion Silvestrini, and Carolina Brito

The Journal of Chemical Physics ARTICLE scitation.org/journal/jcp

Modeling oil–water separation with controlled wetting properties

Cite as: J. Chem. Phys. 154, 104704 (2021); doi: 10.1063/5.0041070
Submitted: 18 December 2020 • Accepted: 17 February 2021 •
Published Online: 8 March 2021

Cristina Gavazzoni,[a] Marion Silvestrini, and Carolina Brito

AFFILIATIONS

Instituto de Física, Universidade Federal do Rio Grande do Sul, Caixa Postal 15051, CEP 91501-970 Porto Alegre, Rio Grande do Sul, Brazil

Note: This paper is part of the JCP Special Collection in Honor of Women in Chemical Physics and Physical Chemistry.
[a]**Author to whom correspondence should be addressed:** crisgava@gmail.com

ABSTRACT

Several oil–water separation techniques have been proposed to improve the capacity of cleaning water. With the technological possibility of producing materials with antagonist wetting behavior, for example, a substrate that repels water and absorbs oil, the understanding of the properties that control this selective capacity has increased with the goal of being used as the mechanism to separate mixed liquids. Besides the experimental advance in this field, less is known from the theoretical side. In this work, we propose a theoretical model to predict the wetting properties of a given substrate and introduce simulations with a four-spin cellular Potts model to study its efficiency in separating water from oil. Our results show that the efficiency of the substrates depends both on the interaction between the liquids and on the wetting behavior of the substrates itself. The water behavior of the droplet composed of both liquids is roughly controlled by the hydrophobicity of the substrate. Predicting the oil behavior, however, is more complex because the substrate being oleophilic does not guarantee that the total amount of oil present on the droplet will be absorbed by the substrate. For both types of substrates considered in this work, pillared and porous with a reservoir, there is always an amount of reminiscent oil on the droplet, which is not absorbed by the substrate due to the interaction with the water and the gas. Both theoretical and numerical models can be easily modified to analyze other types of substrates and liquids.

I. INTRODUCTION

Water separation and purification methods have been widely studied due to environmental, economical, and social issues.[1–4] Particularly, there is an increased level of attention focused in oil–water separation techniques mainly due to oil being the most common pollutant in the world, principally from oil spill accidents and industry oily waste water.[5–7]

Oil/water mixtures can be classified in two different ways depending on the diameter d of the dispersed phase: stratified oil/water ($d > 20\ \mu$m) and emulsified oil/water ($d < 20\ \mu$m).[8] Depending on the type of the mixture, different techniques are used in order to separate oil from water.[9]

Gravity separation followed by skimming is typically used to remove stratified oil from water and is considered an efficient, low cost, and primary step in water treatment.[10,11] For smaller oil droplets, these approaches are not effective, and follow-up steps in treatment are often required. Some of the conventional techniques used to treat emulsions are chemical emulsification,[12] centrifugation,[13,14] heat treatment,[15] and membrane filtration.[3,9] Limitations of these conventional approaches include high energy costs, operating costs, sludge production, and limited efficiency.[7]

Recently, the role of wettability has been studied in order to propose more efficient and low costs water/oil separation methods. The wetting behavior of a certain surface will depend on the geometry and chemistry of the substrate,[16–18] and thus, by controlling these key parameters, one can develop a material with antagonistic wetting behavior for oil and water that propitiates the mixture separation.

With that in mind, several materials with special wetting behavior were developed and successfully applied in oil–water separation. These materials can be classified into oil-removing type of

materials,[19–22] characterized by superhydrophobic/superoleophilic wetting behavior, and water-removing type of materials,[9,23] characterized by superhydrophilic/superoleophobic wetting behavior. Despite the fact that oil-removing materials are more common, they have the disadvantage of being easily fouled by oils due to their oleophilicity nature and have not been suitable for gravity-driven separation due to the higher density of the water. On the other hand, water-removing materials are more difficult to achieve due to the fact that most oleophobic materials are also hydrophobic.[24,25]

Despite all the advances in this field, most of the studies are focused on the fabrication and performance of these materials and not in the underlying mechanisms that propitiate oil/water separation.[8] Therefore, more fundamental research toward understanding the interactions between water, oil, and surfaces is extremely necessary in order to build a robust theoretical background that could be used as a guideline for further developments in this area.

In this work, we address this issue by studying oil/water separation in two distinct oil-removing surfaces: a pillared surface and a porous substrate. We concentrate in the case of small volume droplets, for which the dispersed phase size fits into the range of emulsions, where gravity does not play any role in the separation of oil and water. To do that, we first apply a theoretical continuous model, which takes into account the energy of creating interfaces between solid, liquid, and gas phases when a droplet of pure liquid (water or oil) is placed on a substrate. By applying a minimization procedure, we obtain the wetting state of the droplet that minimizes its energy. This allows us to build a wetting phase diagram for the substrate, which indicates for which range of geometrical parameters the substrate is hydrophobic/oleophilic and the corresponding contact angle of the droplet. To take into account the interaction between water and oil, we simulate a cellular Potts model with four-states using Monte Carlo simulations. It allows us to study the separation capacity of both substrates and evaluate how different geometric parameters affect the performance of these materials in separating oil from water.

This manuscript is organized as follows: In Sec. II, we present the continuous model and discuss the theoretical results. In Sec. III, we introduce the Monte Carlo four-spin cellular Potts model and describe our simulations methods. The simulations results for both surfaces are shown and discussed in Sec. IV. We close this work with our conclusions and possible extensions of our results in Sec. V.

II. THEORETICAL CONTINUOUS MODEL

The goal of this section is to develop a simple model to determine if a given substrate has the capacity to separate water from oil. An ideal oil-removing material is such that when a mixed oil/water droplet is deposited on its surface, the oil penetrates the material and the water remains on its surface. It is then important to identify the wettability states of a substrate.

For this purpose, we first address a following question: if a droplet of fixed volume $V_0 = 4/3\pi R_0^3$ composed by a pure liquid (water or oil) is placed on a rough surface, which is its favorable wetting state? To answer this question, we assume that there are two possible wetting states: one called Wenzel (W) and characterized by the homogeneous wetting of the surface and the other called Cassie–Baxter (CB) with air pockets trapped underneath the droplet. The W state is associated with an omniphilic behavior, while the CB state is associated with an omniphobic one.

In this model, we take into account all the interfacial energies associated with the CB and W states and minimize these energies. The wetting state with minimum energy is the one that is favorable from the energetic viewpoint. Similar ideas were used by other authors,[16,26–28] including two of us.[29–31]

The geometry of the surfaces and the three-dimensional droplet considered in this work is shown in Fig. 1.

The total energy of each of the wetting states is given by the sum of all interfacial energies between the droplet and the desired surface. The energetic difference between the system with and without the droplet is $E^s_{\text{tot}} = \Delta E^s + E^s_g$, where superscript s represents the wetting state (CB or W) and E_g is the gravitational energy. ΔE^s is the difference in the interfacial energy between every pair formed from liquid, solid, and gas after the droplet is placed on the surface in state s and the energy of the surface without the droplet. The importance of the gravitational energy depends on the droplet size and its composition. In this work, we consider droplets with small volumes such that the gravitational energy is negligible compared to ΔE^s.

The interfacial energy equations for pillared substrate, schematized in Fig. 1(a), are developed in Ref. 29 and can be written as

$$\Delta E^{\mathbf{CB}}_{\mathbf{pil}} = \mathrm{N}^{\mathrm{CB}}\left[(\sigma_{\mathrm{SL}} - \sigma_{\mathrm{SG}})\mathrm{w}^2 + (\mathrm{d}^2 - \mathrm{w}^2)\sigma_{\mathrm{GL}}\right] + \sigma_{\mathrm{GL}}\mathrm{S}^{\mathrm{CB}}_{\mathrm{CAP}}, \quad (1)$$

$$\Delta E^{\mathbf{W}}_{\mathbf{pil}} = \mathrm{N}^{\mathrm{W}}\left[(\mathrm{d}^2 + 4\mathrm{hw})\sigma_{\mathrm{SL}}\right] + \sigma_{\mathrm{GL}}\mathrm{S}^{\mathrm{W}}_{\mathrm{CAP}}. \quad (2)$$

For the porous surface schematized in Fig. 1(b), the interfacial energies are given by

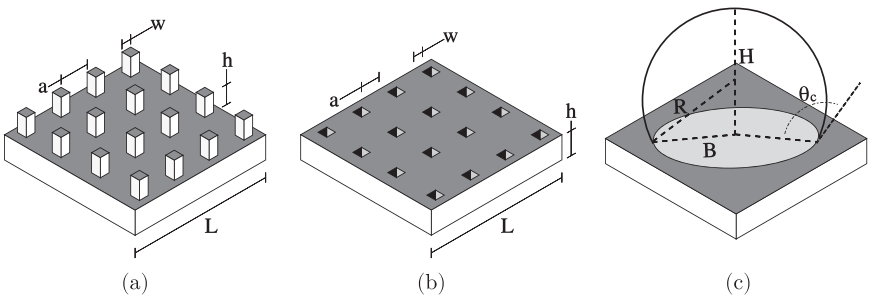

FIG. 1. Definition of the geometric parameters of the substrates and the droplet. (a) Pillared surface with width w, pillar distance *a*, and height h. (b) Porous surface with width w, porous distance *a*, and height h. (c) Geometric parameters of the droplet. We consider a spherical cap with radius *R*, base radius *B*, height *H*, and contact angle θ_C.

TABLE I. Surface tensions used in this work in units of mN/m. These values were obtained for $T = 25\,^{\circ}\mathrm{C}$.

	Water	Solid	Gas
Oil	$\sigma_{WO} = 53.5$	$\sigma_{SO} = 8.6$	$\sigma_{GO} = 27$
Water	⋯	$\sigma_{SW} = 50.2$	$\sigma_{GW} = 70$
Solid	⋯	⋯	$\sigma_{SG} = 25$

$$\Delta E^{CB}_{por} = N^{CB}\left[(d^2 - w^2)(\sigma_{SL} - \sigma_{SG}) + w^2\sigma_{GL}\right] + \sigma_{GL}S^{CB}_{CAP}, \quad (3)$$

$$\Delta E^{W}_{por} = N^{W}\left[(d^2 - w^2 + 4hw)(\sigma_{SL} - \sigma_{SG}) + w^2\sigma_{GL}\right] + \sigma_{GL}S^{W}_{CAP}. \quad (4)$$

For Eqs. (1)–(4), $d = w + a$ and σ_{SG}, σ_{SL}, and σ_{GL} are the surface tensions for the solid–gas, solid–liquid, and liquid–gas interfaces, respectively. The subscript "L" accounts for a liquid phase and can be either water or oil. $N^s = \frac{\pi B^2}{d^2}$ accounts for the number of pillars/pores underneath the droplet and $S_{CAP} = 2\pi R^2[1 - \cos(\theta^s_c)]$ is the surface area of the spherical cap, where $B^s = R^s \sin(\theta^s_c)$ is the base radius and θ^s_c is the contact angle of the droplet, as defined in Fig. 1(c).

In order to identify the favorable wetting state from the thermodynamic point of view for the pillared surface, we minimize Eqs. (1) and (2) and compare the global minimal energy for each state. This energy minimization process goes as follows for the pillared substrate: first, we fix the surface parameters (a, h, and w) and the volume $V_0 = \frac{4}{3}\pi R_0^3$ of the droplet. Next, we solve a cubic equation to obtain the radius of the droplet, R^s, for each state, CB or W. Then, we vary the contact angle $\theta^s_c \in [0, 180^{\circ})$ and use Eq. (1) to obtain ΔE^{CB} and Eq. (2) for ΔE^{W}. It allows us to build a curve of energies as a function of θ^s_c. We find the global minimum energy for CB, ΔE^{CB}_{min}, and for the W state, ΔE^{W}_{min}. The thermodynamic wetting state is the one with the smallest energy. In other words, for example, if $\Delta E^{CB}_{min} > \Delta E^{W}_{min}$, then W is the thermodynamic wetting state. This energy minimization process is explained with further details in Refs. 29 and 30 and we present an example in the supplementary material. For the porous substrate, the process is analogous, but we use Eqs. (3) and (4). Besides predicting the favorable wetting state, this approach also allows the determination of the geometric parameters of the droplet associated with the most stable state, including the contact angle, θ_c.

The continuous model and the minimization process are employed to build a theoretical wetting diagram for both substrates considered in this work. For the calculations, we considered surface tensions obtained from experiments with water droplets on the poly-dimethylsiloxane (PDMS) surface[27] and with hexadecane oil droplets on the same PDMS surface.[32] Solid–liquid surface tensions were obtained from Young's relation $\sigma_{GL}\cos(\theta) = \sigma_{SG} - \sigma_{SL}$, where θ is the contact angle on a smooth surface and assumes the values $\theta^w = 114^{\circ}$ for water[27] and $\theta^{\circ} = 53^{\circ}$ for oil.[32] Water/hexadecane surface tension was obtained from Ref. 33. These surface tensions are summarized in Table I. We fix $w = 5\ \mu$m and screen over the parameters $a \in (0, 16]\ \mu$m and $h \in (0, 15]\ \mu$m.

Figure 2 summarizes our theoretical results for pure water/oil droplets with initial radius $R_o = 50\ \mu$m. We first concentrate in the case of the pillared surface and consider a droplet with pure water. In this case, the surface presents two regions, as shown in Fig. 2(a): for small a and high h, the favorable state is CB, but as the pillar

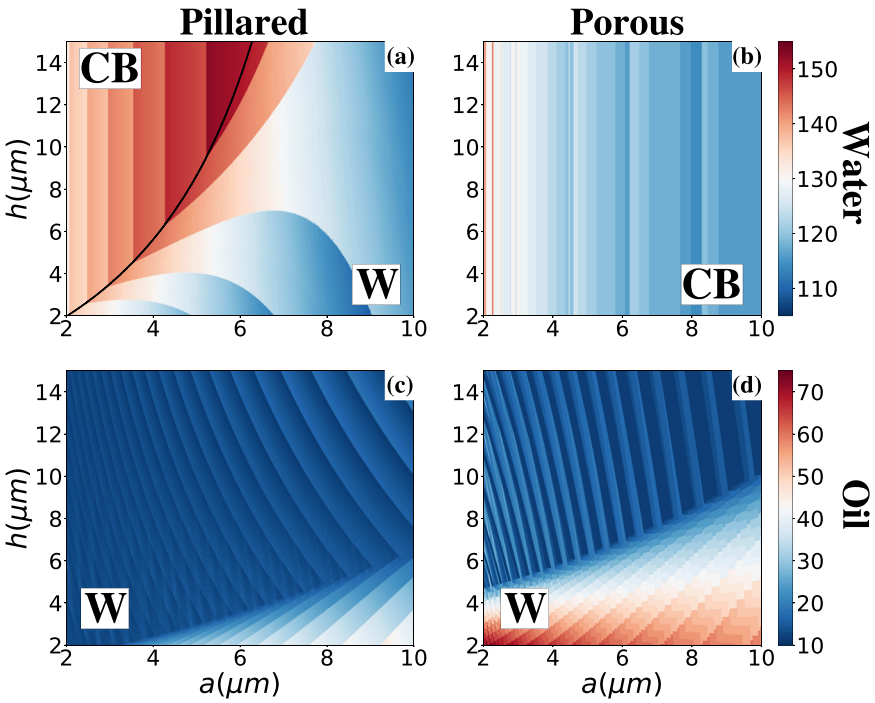

FIG. 2. Theoretical wetting diagrams for (a) the water droplet placed on a pillared surface, (b) water droplet placed on a porous surface, (c) oil droplet placed on a pillared surface, and (d) oil droplet placed on a porous surface as a function of two geometrical parameters of the surface: the height of the pillars h and the interpillar/interporous distance a. Pillar widths are kept constant $w = 5\ \mu$m. The solid line in (a) represents the predicted thermodynamic transition between the Cassie–Baxter (CB) and (W) states. Colors indicate the droplet's contact angle in degrees.

distance, a, increases, a transition to the W state is observed. This transition occurs for different values of a depending on the initial size of the droplet, as shown in Ref. 29. Results for other values of R_o are shown in the supplementary material. When the droplet is composed of pure oil, W is the favorable state for any geometric parameter, as shown in Fig. 2(c).

The same process is applied for the porous substrate. When we consider a droplet of pure water, no phase transition is observed and the favorable wetting state is CB for any geometric parameter, as shown in Fig. 2(b). Nevertheless, lower contact angles were predicted when compared to the pillared surface, indicating that this surface is less hydrophobic. If a droplet of pure oil is taken into account, the thermodynamic state is W in the whole diagram [Fig. 2(d)]. In comparison with the pillared surface, higher values of the contact angle were observed for low values of porous height h.

The analysis presented here indicates that the porous surface could function as a good oil removing material regardless of the choice of the surface geometrical parameters, but higher values of porous height h would favor the separation due to the lower contact angles predicted for the oil droplets. For the pillared surface, we expect a good oil/water separation in the region marked as CB in Fig. 2(a).

However, this approach has the limitation of only considering pure water or pure oil droplets, disregarding the effects of water–oil interaction. In order to overcome this limitation, we perform numerical simulations of the cellular Potts model taking into account the promising interval of parameters obtained by the theoretical analysis discussed in this section.

III. SIMULATIONS: FOUR-SPIN CELLULAR POTTS MODEL

Monte Carlo simulations (MC) of the cellular Potts model have been used to study wetting phenomena in textured surface[34–36] but is also a useful tool to study cell migration on substrates.[37–39] The coarse-grained approach used in these types of simulations (in opposition to the explicit atom approach commonly used in molecular dynamic simulations) is a more consistent framework to treat mesoscopic systems and, therefore, more appropriate for comparison with experimental results.

Here, we expand the 3D cellular Potts model with three states used to simulate the wetting properties of a pure liquid droplet[29,30] to a four-spin model to be able to take into account a droplet composed of a mixture of two liquids: water and oil. Our model consists of a simple cubic lattice in which each state represents one of the components: gas, water, oil, or solid. The Hamiltonian is given by

$$H = \frac{1}{2}\sum_{\langle i,j\rangle} E_{s_i,s_j}(1-\delta_{s_i,s_j}) + \alpha_w\left(\sum_i \delta_{s_i,1} - V_T^w\right)^2 + \alpha_o\left(\sum_i \delta_{s_i,2} - V_T^o\right)^2 + g\sum_i (m_i h_i \delta_{s_i,1} + m_i h_i \delta_{s_i,2}), \quad (5)$$

where the spin $s_i \in \{0, 1, 2, 3\}$ represents gas, water, oil, and solid states, respectively.

The first term in Eq. (5) represents the energy related to the presence of interfaces between sites of different types. The summation ranges over pairs of neighbors, which comprise the 3D Moore neighborhood in the simple cubic lattice (26 sites, excluding the central one), E_{s_i,s_j} is the interaction energies of sites s_i and s_j of different states at interfaces, and δ_{s_i,s_j} is the Kronecker delta.

In the second and third terms in Eq. (5), V_T^w and V_T^o are the target water and oil volumes, respectively, the summations are the water and oil volume, and the parameters α_w and α_o mimic the liquids compressibility. Thus, these terms maintain the liquids' volumes and the desired composition of the droplet constant during the simulation. The last term is the gravitational energy, where $g = 10$ m/s^2 is the acceleration of gravity and m_i is the mass of the site. In both the volumetric and gravitational terms, only sites with liquid, $s_i = 1$ or $s_i = 2$, contribute.

In our simulations, the length scale is such that one lattice spacing corresponds to 1 μm and the surface tensions values (shown in Table I) are divided by 26, which is the number of neighbors that contributes to the first summation of our Hamiltonian. Therefore, the interfacial interaction energies $E_{s_i,s_j} = A\sigma_{s_i s_j}$, with $A = 1\ \mu\text{m}^2$ given by $E_{0,1} = 2.70 \times 10^{-9}$ μJ, $E_{0,2} = 1.04 \times 10^{-9}$ μJ, $E_{0,3} = 0.96 \times 10^{-9}$ μJ, $E_{1,2} = 2.06 \times 10^{-9}$ μJ, $E_{1,3} = 1.93 \times 10^{-9}$ μJ, and $E_{2,3} = 0.33 \times 10^{-9}$ μJ. The mass existent in a unit cube is $m^w = 10^{-15}$ kg for water and $m^o = 0.77 \times 10^{-15}$ kg for oil. We fix $\alpha_w = \alpha_o = 0.01 \times 10^{-9}$ μJ/(μm)^6 (the choice of these values is justified in the supplementary material).

The total run of a simulation is 5×10^5 Monte Carlo steps (MCSs), from which the last 2.5×10^5 MCSs are used to measure observables of interest. Each MCS is composed of $V^T = V^w + V^o$ number of trial spin flips, where V^T is the volume of the liquid droplet, which is composed by a volume of oil V^o and water V^w. A spin flip is accepted with probability $\min\{1, \exp(-\beta\Delta H)\}$, where $\beta = 1/T$. In the cellular Potts model, T acts as noise to allow the phase space to be explored. In our simulations, a value of $T = 9$ was used, which allows an acceptance rate of ~15% while keeping both water and oil in a liquid state (for further information, see the supplementary material).

The initial wetting state is created using a hemisphere with initial volume $V^T \approx V_0 = 4/3\,\pi R_0^3$ due to the discreteness of the lattice. The droplet has $R_0 = 50$ μm in a cubic box with $L = 240$ μm. The composition of the droplet is defined by the oil fraction f_o, and thus, $V^o = f_o V^T$ is the oil volume. One can also define the water volume $V^w = f_w V^T$, where $f_w = 1 - f_o$ is the water fraction. Oil and water sites are randomly distributed in the droplet. As in Sec. II, two different substrates are studied as possible oil-removing materials: pillared surface and porous surface. When the porous surface is used a reservoir with volume, $V_{\text{res}} > 3\ \text{V}^{\text{T}}$ is added to the bottom of the surface, as shown in Fig. 3(b).

A. Definitions of the efficiencies

In order to evaluate the efficiency of the different substrates, we calculated the percentage of the initial oil/water volume that is between the pillars or inside pores, v_p^l, and, for the porous case, the percentage of the initial oil/water volume that is inside the reservoir, v_r^l. The superscription l refers to water, w, or oil, o. Here, we call these quantities *percentage volumes* and they are calculated as follows:

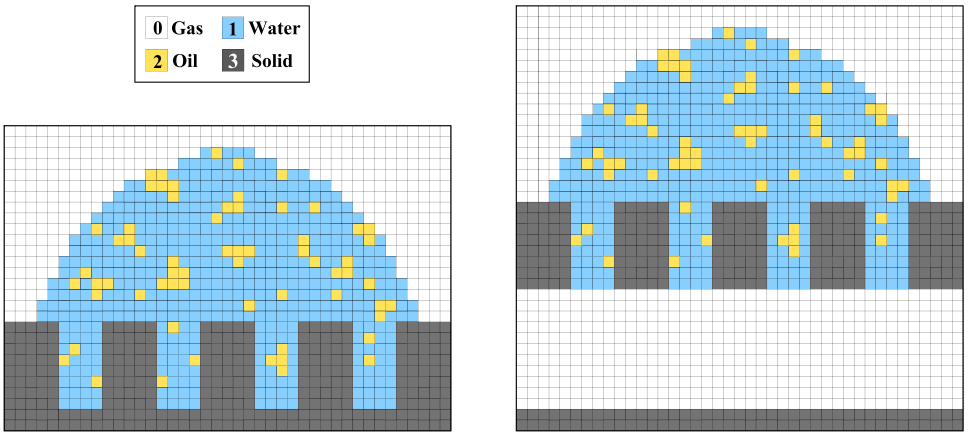

FIG. 3. Visual schematic of the initial setup of the simulations for (a) the pillared surface and (b) the porous surface. Legend shows the label of the spins that represent each state.

$$v_p^l = V_p^l/V^l, \tag{6}$$

$$v_r^l = V_r^l/V^l, \tag{7}$$

where V_p^l is the volume of the liquid (water or oil) between the pillar or inside the pores and V_r^l is the volume of the liquid inside the reservoir. These percentage volumes allow us to define a liquid absorption capacity for the pillared and porous surface that measures how much of the initial liquid volume was absorbed by the substrate,

$$\varepsilon_{\mathbf{pil}}^l = v_p^l, \tag{8}$$

$$\varepsilon_{\mathbf{por}}^l = v_p^l + v_r^l. \tag{9}$$

The ideal substrate for oil and water separation, in our case, is such that all the initial water volume remains above the surface and all the initial oil volume is adsorbed by the substrate. We then introduce a quantity to measure a separation efficiency that takes into account the capacity of a substrate to simultaneously retain the water and absorb the oil,

$$\xi_{\mathbf{S}} = \frac{\varepsilon_{\mathbf{S}}^o + (1 - \varepsilon_{\mathbf{S}}^w)}{2}, \tag{10}$$

where the index S refers to the pillared or porous surface.

We also measure in our simulations two efficiencies that are commonly used in experiments. The first one measures the amount of water that is not absorbed by the substrate.[40,41] In our case, this efficiency is calculated as follows:

$$\xi_{\mathbf{pil}}^{\mathbf{a}} = 1 - v_p^w, \tag{11}$$

$$\xi_{\mathbf{por}}^{\mathbf{a}} = 1 - v_p^w - v_r^w. \tag{12}$$

The second one measures the oil rejection coefficient given by $R = (1 - C_p/C_o)$, where C_o is the initial concentration of oil, which, in our case, is f_o, and C_p is the concentration of oil in the remaining water above the surface.[42,43] In our simulation, this efficiency is calculated as follows:

$$\xi_{\mathbf{pil}}^{\mathbf{r}} = 1 - \left[\frac{V^o - V_p^o}{V^T - [V_p^w + V_p^o]}\frac{1}{f_o}\right], \tag{13}$$

$$\xi_{\mathbf{por}}^{\mathbf{r}} = 1 - \left[\frac{V^o - (V_p^o + V_r^o)}{V^T - [(V_p^w + V_r^w) + (V_p^o + V_r^o)]}\frac{1}{f_o}\right]. \tag{14}$$

IV. RESULTS AND DISCUSSION

In this section, we analyze the simulation results for pillared surfaces [Fig. 1(a)] and porous surfaces, exemplified in Fig. 1(b). We compare these results with the theoretical predictions presented in Sec. II and discuss the efficiency of these two types of surfaces in separating water from oil.

A. Pillared surface

The theoretical results summarized in Fig. 2 show that, if a pure water droplet is placed on a pillared surface, it presents a CB and W regions depending on the substrate's geometrical parameters. As previously explained, these wetting states are associated with hydrophilic and hydrophobic behaviors, respectively. For any geometric parameter, if a pure oil droplet is deposited on the substrate, its favorable state is W, indicating that these substrates are oleophilic. Then, we expect that pillared surfaces could work as an oil removing material in the region where a pure water droplet is in a CB state. If this is the case, these substrates would act as "sponges," absorbing oil and leaving water above the pillars.

With that in mind, here, we study surfaces with fixed pillar height h = 10 μm and pillar width w = 5 μm and several values of pillar distance a. In the supplementary material, we also show the analyses for the case with h = 5 μm, which presents very similar results. Figure 4 shows the interpillar percentage volume, v_p^l, as a function of the pillar distance a for $f_o = 0.10$ [Fig. 4(a)] and $f_o = 0.90$

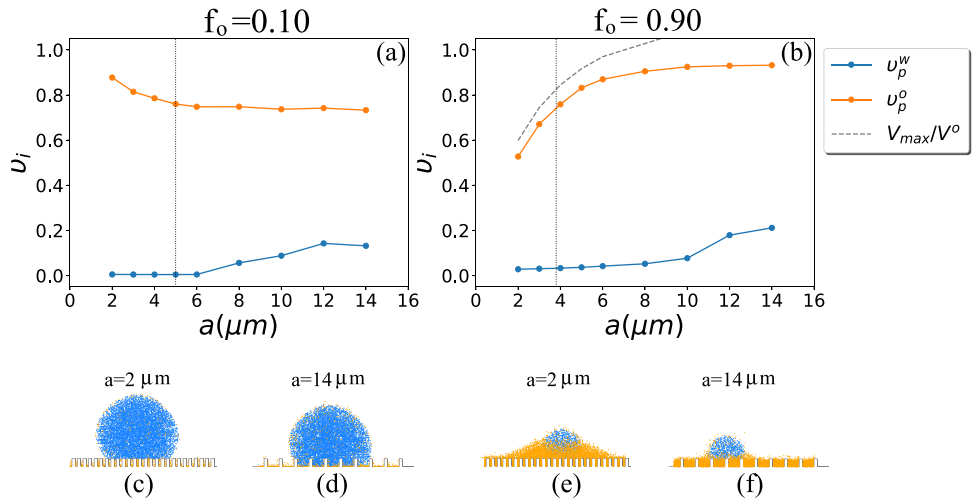

FIG. 4. Results for pillared substrates for several geometric parameters. Top: interpillar volume of water, υ_p^w, and oil, υ_p^o, as a function of the pillar distance a for (a) f_o = 0.10 and (b) f_o = 0.90. Bottom: [(c)–(f)] cross sections of the final droplet configuration of Monte Carlo simulations for a = 2 μm and a = 14 μm for each corresponding f_o. To build this figure, a mixed droplet with oil fraction given by f_o (value specified above the figures) and total volume given by $V^T = 4/3\pi R_0^3$ with R_0 = 50 μm is simulated on a substrate with w = 5 μm, h = 10 μm, and varying pillar distance a. Blue represents water and orange represents oil. Dotted lines represent the CB-W transition predicted by the theoretical model and the dashed line represents the maximum volume available between pillars V_{max} normalized by the total oil volume, V^o.

[Fig. 4(b)] and cross sections of the droplet configuration in the final state of the Monte Carlo simulations corresponding to two different pillar distances, a = 2 μm and a = 14 μm, for each f_o. The vertical gray dotted lines shown in Figs. 4(a) and 4(b) indicate the water CB-W transition predicted by the theoretical continuous model described above for the corresponding water volume. We emphasize that the value of the interpillar distance, a, for which the CB-W transition occurs varies with the droplet initial volume as mentioned previously and is discussed in more detail in the supplementary material.

The available volume to absorb oil is the maximum volume between pillars, given by $V_{\mathbf{max}} = (\frac{L}{d})^2(d^2 - w^2)h$. We normalize this volume by the total oil volume present in the droplet V^o, $V_{\mathbf{max}}/V^o$, and show that this quantity in Fig. 4(b) is represented by the gray dashed line. This curve does not appear for the smaller oil fraction f_o because $V_{\mathbf{max}} \gg V^o$ for all values of a.

For both cases, we observe that for low values of interpillar distance a water does not penetrates the pore, $\upsilon_p^w \approx 0$ [Figs. 4(a) and 4(b)], which is consistent with a CB wetting state. For higher values of the interpillar distance a, we observed an increase in υ_p^w, which roughly coincides with the theoretical prediction from CB to W states indicated by the vertical gray dotted line in Figs. 4(a) and 4(b). This is visually confirmed by the cross sections of the final configurations shown in Figs. 4(c) and 4(d) where the water is in the CB state for a = 2 μm and in the W state for a = 14 μm. We have checked that it also happens for f_o = 0.9 [Figs. 4(e) and 4(f)], but it is not possible to visualize because the oil sites dominate the image and do not allow us to properly see the water behavior.

Although we obtain good agreement with the theoretical results for the water behavior, we note that, when considering the mixture, the phase transition occurs for higher values of the interpillar distance a. This discrepancy is expected because the wetting diagram, obtained by the theoretical continuous model, is built for a pure water droplet or pure oil droplet, while in the simulations, there is a composition of both liquids.

We now discuss the oil behavior. Theoretical calculations show that a pure oil droplet does not undergo any wetting state transition, remaining in the W state for all values of interpillar distance a. This is qualitatively confirmed by simulations, as shown by the oil penetration in Figs. 4(a) and 4(b). For f_o = 0.10 [Fig. 4(a)] and low values of the interpillar distance, a υ_p^o indicates that 88% of the initial oil volume penetrates the substrate. As a is increased, the percentage decreases and a plateau is observed at $\upsilon_p^o \approx 0.73$. For the case with f_o = 0.9, we observe an increase in υ_p^o with the increase in a and a plateau is reached at $\upsilon_p^o \approx 0.93$. This change in the oil absorption behavior is due to the substrate available volume, $V_{\mathbf{max}}$. For lower values of the interpillar distance, a, the pillared surface has space to accommodate roughly 60% of the initial oil volume, as indicated by the gray dashed line, resulting in a reduced oil absorption capacity and the saturation of the substrate. Increasing the interpillar distance a also increases the available volume, $V_{\mathbf{max}}$, and a better oil absorption capacity is observed.

Despite the high percentage of the oil absorbed by the surface, we note that from 7% to 27% of the initial oil remains above the surface. We have checked that all the remaining oil is at the interface of the droplet, which creates a water–oil–gas interface. We note that reminiscent oil in the remaining water was also observed experimentally.[44,45]

To understand this feature in our simulations, we analyzed the terms of Eq. (5) related to the energy for creating interfaces and evaluated the necessary conditions for the appearance of a spin of type "oil" on the interface between the water and the gas. The calculations

and more detailed arguments are discussed in the supplementary material. This analysis led to two main conclusions: (i) the presence of an oil site on the interface of the droplet is favored when there are other oil sites surrounding it, suggesting that in the experiment, the oil would form a film on the interface of the droplet and (ii) the formation of the oil film prevents a water–gas interface that is energetically unfavorable due to the σ_{GW}–σ_{WO} relation due to the fact that $\sigma_{GW} > \sigma_{WO}$. This suggests that changing the surrounding gas in order to change the surface tensions relation may benefit the separation of oil and water.

To conclude this section, we discuss the efficiency of this type of substrate using three different definitions introduced in Sec. III. We measure ξ^{a}_{pil}, defined in Eq. (11), which measures the amount of water that is not absorbed by the surface, and ξ^{r}_{pil}, defined in Eq. (13), which measures the capacity of the surface to exclude oil from the water that remains above the surface. We compare these quantities with the proposed separation efficiency given by Eq. (10), which takes into account both the capacity of maintaining water above the substrate and the capacity of absorbing oil.

Figure 5 summarizes our results for all geometries considered here. For both values of f_o, ξ^{a}_{pil} follows the behavior of water: it shows high efficiency when the water is in the CB state and decays when the transition to W occurs. The ξ^{r}_{pil}, on the other hand, follows roughly the behavior of the oil where the efficiency is high for surfaces where the oil percentage volume v^{o}_{p} is also high.

These definitions of efficiency have the disadvantage of only considering one aspect of the separation process, which is the absorption of the oil *or* the amount of water remaining above the surface. For instance, let us consider the case of $f_o = 0.90$ and $a = 2\ \mu$m. ξ^{a}_{pil} indicates an efficiency of this substrate of ~100% despite the fact that about 50% of the oil remains above the surface, as shown in Fig. 4(e). In other words, ξ^{a}_{pil} is high because there is no absorption of water by the substrate, but it is misleading because if the oil remains above the surface too, then the separation of water and oil is not as good as its high value may suggest at the first glance. On the other hand, ξ^{r}_{pil} has a low value despite the fact that almost the whole amount the initial water remains above the substrate.

The definition of efficiency ξ_{pil} introduced in this work for oil removing materials takes into account both the water retention above the substrate *and* the oil absorption, which are the mechanisms that contribute to the water/oil separation. Thus, considering the same case of $f_o = 0.90$ and $a = 2\ \mu$m discussed above, ξ_{pil} is lower than ξ^{a}_{pil} because it considers the reminiscent oil above the surface and ξ_{pil} is greater than ξ^{r}_{pil} because it considers the quantity and purity of the absorbed oil.

Despite the good efficiency observed for some these pillared surface, they have the limitation of only being able to absorb a certain volume of oil, V_{max}. In Sec. IV B, we evaluate the performance of a surface that, in principle, does not have this problem.

B. Porous surface

In this section, we consider a porous substrate where the oil can be drained into a reservoir. Here, we explore this surface for the same oil fractions f_o and similar geometrical parameters considered for the pillared surface: w = 5 μm, h = 10 μm, and several values of porous distance a. According to the theoretical predictions, for pure water or pure oil, there is no wetting transition: the porous surface is hydrophobic and oleophilic for all values of geometric parameters, as summarized in Figs. 2(b) and 2(d).

Figure 6 shows the interporous percentage volume v^{l}_{p} and the reservoir percentage volume v^{l}_{r} as a function of porous distance a for two oil fractions, $f_o = 0.10$ and 0.90. For this type of surface, the volume normalization is such that $V^{l}_{p} + V^{l}_{r} + V^{l}_{a} = V^{l}$, where V^{l}_{a} is the remaining volume above the surface. For water, we observe that $v^{w}_{p} \approx 0$ and $v^{w}_{r} \approx 0$ for all geometric parameters and oil fractions considered here, which means that water remains above the surface and does not enter the porous or the reservoir for both values of f_o and all values of a. This is in agreement with the theoretical predictions for pure water on porous substrates shown in Fig. 2(b), which indicates that they are hydrophobic for all geometric parameters.

Concerning the oil behavior, Fig. 6 shows its presence in the pores v^{o}_{p} and in the reservoir v^{o}_{r} separately and also the sum of both contributions. The available volume to absorb oil for the porous case is given by $V_{max} = (\frac{L}{d})^2 hw^2$. This quantity is normalized by the initial oil volume in the droplet and is represented in Fig. 6 by a dashed line.

Two things dictate the oil behavior for the porous surface: (i) the available volume inside the pores and (ii) the solid surface area above and below the substrate. For small values of the porous distance a, we have more interporous volume available for the oil and a smaller solid surface above and below the substrate, and thus, the oil remains inside the pores. As a is increased, v^{o}_{p} decreases due to the limited volume of the porous and v^{o}_{r} increases due to the increase in

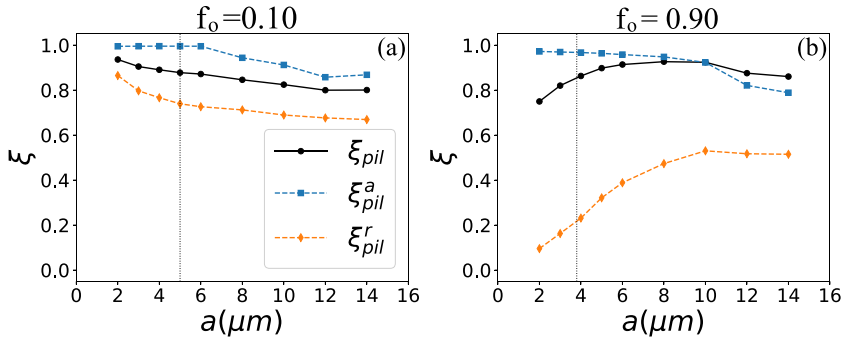

FIG. 5. Efficiency for pillared substrates. ξ^{a}_{pil}, ξ^{r}_{pil}, and ξ_{pil} as a function of the interpillar distance a for (a) $f_o = 0.10$ and (b) $f_o = 0.90$. Dotted lines represent the CB-W transition predicted by the theoretical model.

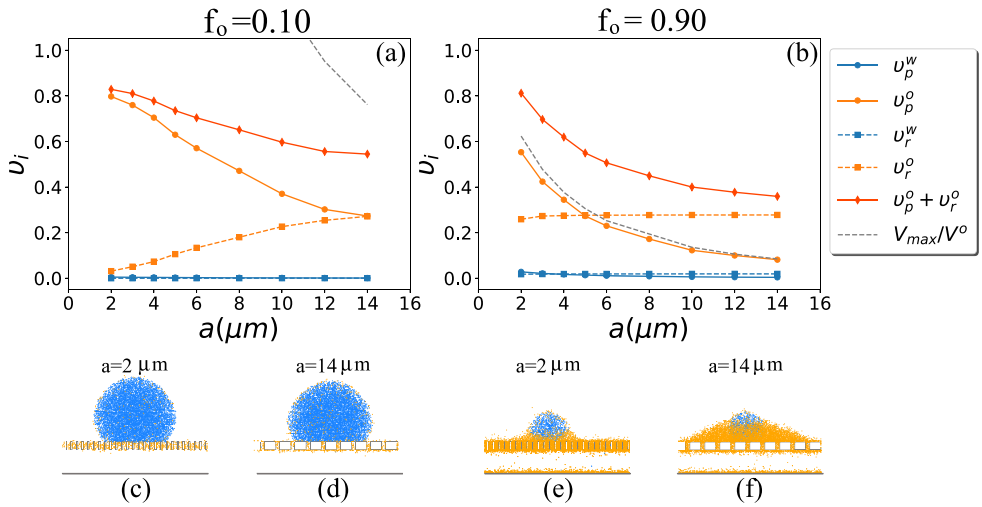

FIG. 6. Results for porous substrates for several geometric parameters. Top: interporous volume of water υ_p^w and oil υ_p^o and reservoir volume of water υ_r^w and oil υ_r^o as a function of the pillar distance a for (a) $f_o = 0.10$ and (b) $f_o = 0.90$. Bottom: [(c)–(f)] cross sections of the final droplet configuration of Monte Carlo simulations for $a = 2$ μm and $a = 14$ μm for each corresponding f_o. To build this figure, a mixed droplet with oil fraction given by f_o (value specified above the figures) and volume given by $V^T = 4/3\pi R_0^3$ with $R_0 = 50$ μm is simulated on a substrate with w = 5 μm, h = 10 μm, and varying porous distance a. Blue represents water and orange represents oil. Dashed lines represent the maximum volume available between porous V_{max} normalized by the total oil volume, V^o.

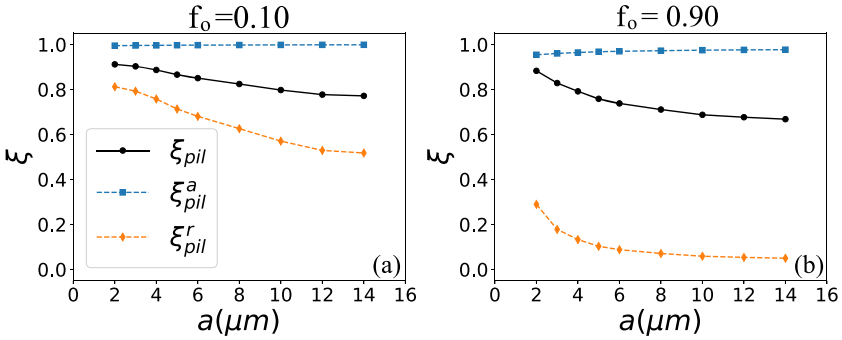

FIG. 7. Results for porous substrates. ξ^a_{por}, ξ^r_{por}, and ξ_{por} as a function of interpillar distance a for (a) $f_o = 0.10$ and (b) $f_o = 0.90$.

the solid surface. However, the increase in the solid surface allows for the formation of an oil film on the surface as well, which jeopardizes the entry of the oil in the reservoir. Since gravity does not play any role for this volume size, once the porous are filled with oil, it creates a layer that prevents the rest of the oil present above the substrate to be absorbed and stored in the reservoir. The formation of a film in the interface between water and gas is also observed for the porous surface. The existence of this film was discussed in Sec. IV A and in the supplementary material.

Figure 7 shows the efficiency of these surfaces in terms of the three measures defined previously in Eqs. (10), (12), and (14). Similar to the discussion we did for the pillar substrates, ξ^a_{por} and ξ^r_{por} follow the behavior of the water and oil absorption, respectively. In other words, these quantities only reflect the hydrophobicity or oleophilicity of the substrate and, therefore, ignore part of the relevant mechanisms involved in water/oil separation. The alternative definition ξ_{por} takes into account both the hydrophobicity and oleophilicity by considering the total oil present in the droplet to define efficiency, allowing us to have an idea of the reminiscent oil above besides the information about the amount of water below the substrate.

V. CONCLUSIONS

In this work, we propose a theoretical and a numerical model to investigate the efficiency of a substrate in separating oil from water by controlling its wetting properties. We apply these methods in pillared and porous substrates. We first used the theoretical model[29,30] to investigate the wetting behavior of the substrate when a droplet of pure oil or water is deposited on it. This approach takes into account the energy of creating interfaces between the liquid, the gas, and the solid and employs a minimization procedure to obtain the thermodynamic wetting state of a droplet, together with a determination of

its contact angle. With this method, we built a wetting state diagram of the substrates, which indicates the range of geometric parameters for which the substrate is hydrophobic or oleophilic. With the idea that an appropriate material to separate oil from water would be oleophilic and hydrophobic, this diagram guides us in choosing the adequate type of substrate and its range of geometrical parameters. Because the theoretical approach does not take into account the interaction between water and oil, we introduced a four-state Potts model and implemented Monte Carlo simulations to study the efficiency of the substrates in separating water from oil at different proportions of both liquids.

The theoretical analyses show that pillared substrates present a hydrophobic and a hydrophilic phase [Fig. 2(a)] and are oleophilic for all geometric parameters [Fig. 2(c)]. The porous substrates are hydrophobic and oleophilic for all geometric parameters [Figs. 2(a) and 2(c)]. We then simulated a droplet with fixed volume size but different oil fractions on both types of substrates. In this work, we concentrate on the case where the droplet is small enough to guarantee that gravity is not relevant compared to the energy scales of the interfacial energies. Overall, our simulation results shown in Figs. 4 and 6 allow us to conclude that the water behavior of the mixed droplet can be explained by the hydrophobicity of the substrate, but the oil behavior is more complex than just evaluating if the substrate is oleophilic. In other words, if the substrate is hydrophobic when tested with pure water, when a mixed droplet composed of water and oil is deposited on it, water remains above the substrate. Predicting the oil behavior is more difficult because the absorption capacity of the surfaces is limited for two reasons: (i) some part the oil remains on the droplet, forming a film between the water and the gas phase, and (ii) in the absence of gravity, once the substrate is filled with the oil, even in the presence of a reservoir (which is the case of our porous substrate), the oil does not fill it completely.

Concerning the efficiency of the substrates in separating water from oil, in the literature, there are some ways to define it and the goodness of the definition depends on what is aimed to capture. In this work, we investigated three different definitions of efficiency: ξ^a measures the percentage of water that remains above the substrate, ξ^r measures the percentage of oil absorbed by the substrate, and ξ measures the capacity of *simultaneously* retaining the water and absorbing the oil. We compared these tree quantities for different geometries of substrates and showed that, for a given substrate, these efficiencies present different values. Since the definition of the efficiency varies in different works,[8] comparisons between different experimental works should be done carefully.

Both theoretical and simulations models can be modified to analyze other types of substrates and to take into account some effects that are not considered in this work. We discuss some examples and their interests in the following. We studied in this work situations where the mass of oil is small enough for gravity not being relevant, which is the case for emulsions, for example. For these situations, a superhydrophobic fractal substrate[46,47] could act as an efficient sponge to absorb oil from water because it maximizes the contact surface between oil and the solid. We could also analyze the situation where the volume of oil is bigger and gravity would be an important element. This can be introduced in our model by changing the length scale for the sites and it would allow us to access phenomena that happen in free oil/water mixtures and dispersion. Another possible adaptation of this model is the study of underwater wetting phenomena, which can be of practical interest if the separation of oil and water happens without a presence of gas.[8,9]

SUPPLEMENTARY MATERIAL

See the supplementary material for a detailed description and an example of the energy minimization process for the continuous model, the methodology used in choosing the numerical parameters, and supplementary results.

DEDICATION

This paper is dedicated to Professor Marcia Cristina Bernardes Barbosa, an outstanding Brazilian physicist who not only has greatly contributed to our knowledge of the water behavior but also actively acts against gender inequality in the field. She inspires many women, including the authors of this manuscript, to pursue a scientific career.

ACKNOWLEDGMENTS

We thank the Brazilian agency CAPES and CNPq for the financial support.

DATA AVAILABILITY

The data that support the findings of this study are available within the article and its supplementary material.

REFERENCES

[1] M. M. Mekonnen and A. Y. Hoekstra, "Four billion people facing severe water scarcity," Sci. Adv. **2**, e1500323 (2016).
[2] H.-H. Huang, R. K. Joshi, K. K. H. De Silva, R. Badam, and M. Yoshimura, "Fabrication of reduced graphene oxide membranes for water desalination," J. Membr. Sci. **572**, 12–19 (2019).
[3] Y. Yang, X. Yang, L. Liang, Y. Gao, H. Cheng, X. Li, M. Zou, R. Ma, Q. Yuan, and X. Duan, "Large-area graphene-nanomesh/carbon-nanotube hybrid membranes for ionic and molecular nanofiltration," Science **364**, 1057–1062 (2019).
[4] Y. Qian, X. Zhang, C. Liu, C. Zhou, and A. Huang, "Tuning interlayer spacing of graphene oxide membranes with enhanced desalination performance," Desalination **460**, 56–63 (2019).
[5] Z. Xue, Y. Cao, N. Liu, L. Feng, and L. Jiang, "Special wettable materials for oil/water separation," J. Mater. Chem. A **2**, 2445–2460 (2014).
[6] Y. J. Chan, M. F. Chong, C. L. Law, and D. G. Hassell, "A review on anaerobic–aerobic treatment of industrial and municipal wastewater," Chem. Eng. J. **155**, 1–18 (2009).
[7] M. Padaki, R. Surya Murali, M. S. Abdullah, N. Misdan, A. Moslehyani, M. A. Kassim, N. Hilal, and A. F. Ismail, "Membrane technology enhancement in oil–water separation: A review," Desalination **357**, 197–207 (2015).
[8] C. Chen, D. Weng, A. Mahmood, S. Chen, and J. Wang, "Separation mechanism and construction of surfaces with special wettability for oil/water separation," ACS Appl. Mater. Interfaces **11**, 11006–11027 (2019).
[9] A. K. Kota, G. Kwon, W. Choi, J. M. Mabry, and A. Tuteja, "Hygro-responsive membranes for effective oil–water separation," Nat. Commun. **3**, 1025 (2012).

[10]M. Cheryan and N. Rajagopalan, "Membrane processing of oily streams. Wastewater treatment and waste reduction," J. Membr. Sci. **151**, 13–28 (1998).
[11]J. A. Zeevalkink and J. J. Brunsmann, "Oil removal from water in parallel plate gravity-type separators," Water Res. **17**, 365–373 (1983).
[12]D. Sun, X. Duan, W. Li, and D. Zhou, "Demulsification of water-in-oil emulsion by using porous glass membrane," J. Membr. Sci. **146**, 65–72 (1998).
[13]A. Cambiella, J. M. Benito, C. Pazos, and J. Coca, "Centrifugal separation efficiency in the treatment of waste emulsified oils," Chem. Eng. Res. Des. **84**, 69–76 (2006).
[14]M. Comba and K. Kaiser, "Suspended particulate concentrations in the St. Lawrence river (1985–1987) determined by centrifugation and filtration," Sci. Total Environ. **97-98**, 191–206 (1990).
[15]T. Strøm-Kristiansen, A. Lewis, P. S. Daling, and A. B. Nordvik, "Heat and chemical treatment of mechanically recovered w/o emulsions," Spill Sci. Technol. Bull. **2**, 133–141 (1995).
[16]D. Quéré, "Wetting and roughness," Annu. Rev. Mater. Res. **38**, 71–99 (2008).
[17]R. N. Wenzel, "Resistance of solid surfaces to wetting by water," Indust. Eng. Chem. **28**, 988–994 (1936).
[18]R. N. Wenzel, "Surface roughness and contact angle," J. Phys. Chem. **53**, 1466–1467 (1949).
[19]L. Feng, Z. Zhang, Z. Mai, Y. Ma, B. Liu, L. Jiang, and D. Zhu, "A super-hydrophobic and super-oleophilic coating mesh film for the separation of oil and water," Angew. Chem., Int. Ed. **43**, 2012–2014 (2004).
[20]X. Gui, J. Wei, K. Wang, A. Cao, H. Zhu, Y. Jia, Q. Shu, and D. Wu, "Carbon nanotube sponges," Adv. Mater. **22**, 617–621 (2010).
[21]B. Cortese, D. Caschera, F. Federici, G. M. Ingo, and G. Gigli, "Superhydrophobic fabrics for oil–water separation through a diamond like carbon (DLC) coating," J. Mater. Chem. A **2**, 6781–6789 (2014).
[22]Y. Zhan, S. He, J. Hu, S. Zhao, G. Zeng, M. Zhou, G. Zhang, and A. Sengupta, "Robust super-hydrophobic/super-oleophilic sandwich-like UIO-66-F_4@rGO composites for efficient and multitasking oil/water separation applications," J. Hazard. Mater. **388**, 121752 (2020).
[23]J. Yang, Z. Zhang, X. Xu, X. Zhu, X. Men, and X. Zhou, "Superhydrophilic–superoleophobic coatings," J. Mater. Chem. **22**, 2834–2837 (2012).
[24]A. Tuteja, W. Choi, M. Ma, J. M. Mabry, S. A. Mazzella, G. C. Rutledge, G. H. McKinley, and R. E. Cohen, "Designing superoleophobic surfaces," Science **318**, 1618–1622 (2007).
[25]A. Ahuja, J. A. Taylor, V. Lifton, A. A. Sidorenko, T. R. Salamon, E. J. Lobaton, P. Kolodner, and T. N. Krupenkin, "Nanonails: A simple geometrical approach to electrically tunable superlyophobic surfaces," Langmuir **24**, 9–14 (2008).
[26]M. Sbragaglia, A. Peters, C. Pirat, B. Borkent, R. Lammertink, M. Wessling, and D. Lohse, "Spontaneous breakdown of superhydrophobicity," Phys. Rev. Lett. **99**, 156001 (2007).
[27]P. Tsai, R. Lammertink, M. Wessling, and D. Lohse, "Evaporation-triggered wetting transition for water droplets upon hydrophobic microstructures," Phys. Rev. Lett. **104**, 116102 (2010).
[28]A. Shahraz, A. Borhan, and K. A. Fichthorn, "A theory for the morphological dependence of wetting on a physically patterned solid surface," Langmuir **28**, 14227–14237 (2012).
[29]H. C. M. Fernandes, M. H. Vainstein, and C. Brito, "Modeling of droplet evaporation on superhydrophobic surfaces," Langmuir **31**, 7652–7659 (2015).
[30]M. Silvestrini and C. Brito, "Wettability of reentrant surfaces: A global energy approach," Langmuir **33**, 12535–12545 (2017).
[31]D. Lazzari and C. Brito, "Geometric and chemical nonuniformity may induce the stability of more than one wetting state in the same hydrophobic surface," Phys. Rev. E **99**, 032801 (2019).
[32]S. Martin and B. Bhushan, "Transparent, wear-resistant, superhydrophobic and superoleophobic poly(dimethylsiloxane) (PDMS) surfaces," J. Colloid Interface Sci. **488**, 118–126 (2017).
[33]D. Wu and V. Hornof, "Dynamic interfacial tension in hexadecane/water systems containing ready-made and *in-situ-formed* surfactants," Chem. Eng. Commun. **172**, 85–106 (1999).
[34]D. M. Lopes, S. M. M. Ramos, L. R. de Oliveira, and J. C. M. Mombach, "Cassie-Baxter to Wenzel state wetting transition: A 2D numerical simulation," RSC Adv. **3**, 24530–24534 (2013).
[35]L. R. de Oliveira, D. M. Lopes, S. M. M. Ramos, and J. C. M. Mombach, "Two-dimensional modeling of the superhydrophobic behavior of a liquid droplet sliding down a ramp of pillars," Soft Matter **7**, 3763–3765 (2011).
[36]V. Mortazavi, R. M. D'Souza, and M. Nosonovsky, "Study of contact angle hysteresis using the cellular Potts model," Phys. Chem. Chem. Phys. **15**, 2749–2756 (2013).
[37]F. Graner and J. A. Glazier, "Simulation of biological cell sorting using a two-dimensional extended Potts model," Phys. Rev. Lett. **69**, 2013–2017 (1992).
[38]I. Fortuna, G. C. Perrone, M. S. Krug, E. Susin, J. M. Belmonte, G. L. Thomas, J. A. Glazier, and R. M. de Almeida, "CompuCell3D simulations reproduce mesenchymal cell migration on flat substrates," Biophys. J. **118**, 2801 (2020).
[39]R. Magno, V. A. Grieneisen, and A. F. Marée, "The biophysical nature of cells: Potential cell behaviours revealed by analytical and computational studies of cell surface mechanics," BMC Biophys. **8**, 8 (2015).
[40]J. Gu, P. Xiao, J. Chen, F. Liu, Y. Huang, G. Li, J. Zhang, and T. Chen, "Robust preparation of superhydrophobic polymer/carbon nanotube hybrid membranes for highly effective removal of oils and separation of water-in-oil emulsions," J. Mater. Chem. A **2**, 15268–15272 (2014).
[41]A. K. Singh and J. K. Singh, "Fabrication of zirconia based durable superhydrophobic–superoleophilic fabrics using non fluorinated materials for oil–water separation and water purification," RSC Adv. **6**, 103632–103640 (2016).
[42]Z. Wang, C. Xiao, Z. Wu, Y. Wang, X. Du, W. Kong, D. Pan, G. Guan, and X. Hao, "A novel 3D porous modified material with cage-like structure: Fabrication and its demulsification effect for efficient oil/water separation," J. Mater. Chem. A **5**, 5895–5904 (2017).
[43]M. Su, Y. Liu, S. Li, Z. Fang, B. He, Y. Zhang, Y. Li, and P. He, "A rubber-like, underwater superoleophobic hydrogel for efficient oil/water separation," Chem. Eng. J. **361**, 364–372 (2019).
[44]M. A. Gondal, M. S. Sadullah, M. A. Dastageer, G. H. McKinley, D. Panchanathan, and K. K. Varanasi, "Study of factors governing oil–water separation process using TiO_2 films prepared by spray deposition of nanoparticle dispersions," ACS Appl. Mater. Interfaces **6**, 13422–13429 (2014).
[45]Y. Liu, K. Zhang, W. Yao, C. Zhang, Z. Han, and L. Ren, "A facile electrodeposition process for the fabrication of superhydrophobic and superoleophilic copper mesh for efficient oil–water separation," Ind. Eng. Chem. Res. **55**, 2704–2712 (2016).
[46]T. Onda, S. Shibuichi, N. Satoh, and K. Tsujii, "Super-water-repellent fractal surfaces," Langmuir **12**, 2125–2127 (1996).
[47]A.-L. Barabási and H. E. Stanley, *Fractal Concepts in Surface Growth* (Cambridge University Press, 1995).